Determine Disturbance Locations in Power Grids using Bicubic 2D Interpolation on Electromechanical Wave-front Propagation Delay

Shutang You

Abstract: This study presents a method to locate power system disturbance using wide-area synchrophasor measurements. The merits of the proposed method include robustness and easy for visualization. In addition, the proposed method facilitates the calculation of electromechanical wave propagation speed distribution. An example of locating the disturbance and generating the propagation speed distribution is demonstrated based on FNET/GridEye, a distribution-level wide-area measurement system. Without losing generality, the proposed method can be implemented in any other wide-area measurement systems.

1. Introduction

As renewable generation increases, due to system uncertainty and complexity, modern power system operation increasingly relies on high-resolution real-time situation awareness systems [1-6]. Wide-area synchrophasor measurement systems (WAMS) can provide measurements with a much higher time resolution than conventional measurement systems. Therefore, WAMS is considered as the state-of-the-art technology to monitor power grid dynamics [7, 8]. The utility-level sensor in WAMS is called Phasor Measurement Units (PMU). PMUs are expensive, installed in high voltage environments, and need complex installation and maintenance procedures, which hinder their deployment substantially. Also, PMU measurement is considered as property data, which makes it difficult for exchanging between utility companies [9-19].

As the WAMS deployed at the distribution level, FNET/GridEye has been monitoring power grids using synchrophasor technology for more than 10 years [20-43]. Measured data include frequencies, voltage phasor angles and magnitudes, as well as power quality data. FNET/GridEye consists of two major parts: over 300 frequency disturbance recorders (FDRs) as the sensors installed on world-wide power grids, and the data centre hosted at the University of Tennessee, Knoxville (UTK) and Oak Ridge National Laboratory (ORNL). As a quickly-deployable distribution-level synchrophasor measurement system, multiple applications have been developed [14, 37, 44-47]. Compared with WAMSs owned by utilities, FNET/GridEye has many unique applications. One of such applications is disturbance location determination.

Power grids are subjected to various types of disturbances frequently, such as load variations, generator and line trip, and faults. Many disturbances are minor but large disturbances or events may lead to system emergency states [48-64]. Automatic event detection and locating events can improve situation awareness and activate appropriate controls to prevent cascading failures. Taking the generation trip location

as an example, detecting a generation trip event will allow demand side frequency response. Further, locating a generation trip will allow each balancing authority to minimize frequency excursions and constrain the impact of the event through proper frequency control strategies, such as activating system reserve and leveraging responsive loads.

The type of event can be identified based on the footprints on the frequency or angle profiles. In the FNET/GridEye system, different types of events will have unique characteristics on the frequency measurements. For example, typical load shedding will cause a sharp increase on the frequency profile, while generator disconnection will result to a sharp frequency decrease. Line trip events will cause oscillations on frequency but without change on the average frequency. A fault event will cause a relatively local frequency drop. These features can be used to detect different types of events, as investigated in [65, 66].

This paper mainly focuses on the event location problem. Existing disturbance locating methods have two major steps: obtaining the FDR response time and estimating the location. The FDR response time can be obtained using the time of the frequency measurement passing a threshold. For estimating the disturbance location, the least-square disturbance location approach needs the assumption that the electromechanical wave propagation speed is already known and keeps constant throughout the system [67]. Otherwise, the method will give a series of suspicious locations: one location for each propagation speed. However, in practice, there does not exist a uniform speed that is always valid for one power grid. Actually, the propagation speed varies with the system conditions such as unit commitment and load dynamics, making the approach difficult to be applied. The method described in [68] combines power grid models and measurements to locate generator trips. However, this method heavily relies on the power grid model in calculating the propagation distance. This model-dependency makes it not applicable when the model is not available or the system topology changes with operation conditions. Ref. [69] described a non-parametric approach. This approach determines the likelihood of event location by partition the plane into two parts for each two measurements. The result of this approach may give large and irregular areas as suspicious locations of a disturbance and it is sometimes hard to choose the probability distribution function.

In summary, existing disturbance location approaches either relies on system models or are highly depend on parameters [70]. This paper presents a robust and parameter-insensitive method to locate disturbance location based on FNET/GridEye. To pinpoint the event location, this method combines the Delaunay triangulation [71, 72] and the bicubic 2D interpolation [73] by reconstructing the wave arrival time. In addition, under the framework of the proposed method, it is convenient to calculate the disturbance

propagation speed distribution in the power grid, which is valuable information to ensure reliable protection actions under high renewable penetrations [2, 74, 75].

The rest of this paper is organized as follows: Sections 2 gives an overview on the FNET/GridEye system. Section 3 describes the new event location method and its implementation in FNET/GridEye. Conclusions are presented in Section 4.

2. Overview On FNET/GridEye, A Distribution-Level Wide-Area Measurement System

2.1. Frequency Disturbance Recorder

The idea of distribution-level synchrophasor technology makes it possible to significantly decrease WAMS costs and simply deployment [76]. Nevertheless, special technical challenges arise when designing hardware and software for synchrophasor measurement sensors in the distribution system [77]. For example, different from transmission systems, distribution systems have much worse power quality due to the harmonics and distortions produced by various electric appliances. Under these circumstances, the distribution-level sensors should be capable to capture power grid dynamics at noisy system ends.

Embedded with a microprocessor for sampling and estimating frequency and voltage phasor, as well as other modules for GPS time synchronization and Ethernet communication, FDR features low manufacturing cost, which is about one tenth of a typical PMU [78]. Besides, FDR simplifies installation procedures to plug-and-play. FDR does not sacrifice its accuracy for low cost and quick deployment [79]. In fact, FDR has comparable or even higher accuracy than its counterparts. For example, the target of Micro-FDR is $\pm 0.05\,^\circ$ in angle measurement accuracy, which is surpassed by FDR [80]. So far, three generations of FDRs have been developed for improved measurement accuracy and data quality. Fig.1 shows the most widely deployed Generation-II FDR. Updates on Generation-III FDR include enhanced functionalities on power quality measurements, and more importantly, accuracy improvement archived by hardware and algorithm advancement. Its measurement accuracy reaches a record of ± 0.00006 Hz (for frequency) and $\pm 0.003\,^\circ$ (for voltage angle) under steady states.

Fig. 1. *Generation-II FDR*

The deployment of FDR in North America and its FNET/GridEye world-wide coverage by 2015 are shown in Fig.2 and Fig.3, respectively. Real-time phasor measurements collected by FDRs at the indicated locations are transmitted via Ethernet and collected by the data centre hosted at UTK and ORNL. These measurements enable performing multiple functionalities including online monitoring, online analysis, and offline data mining, revealing valuable insights into power grid dynamic behaviours.

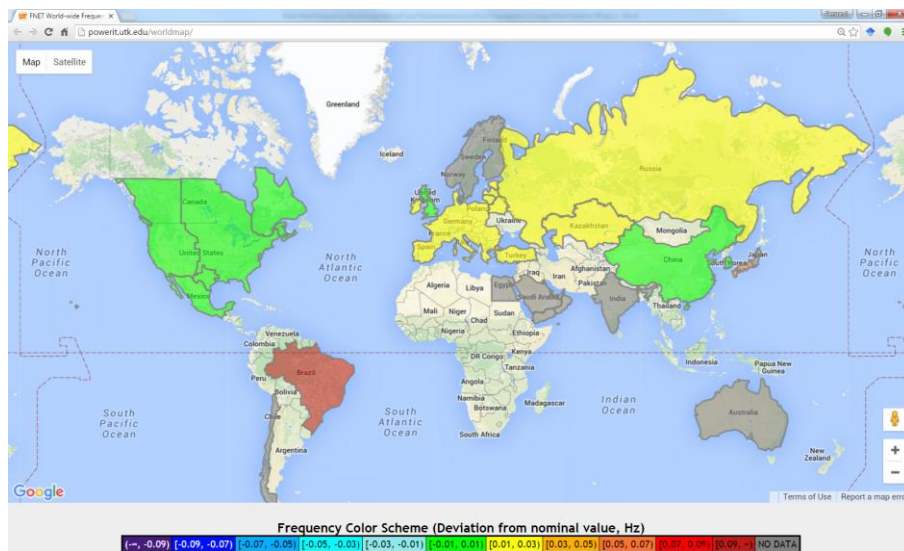**Fig. 2.** *The FDR location map in North America*

Fig. 3. *World-wide FDR deployment and the frequency map*

2.2. FNET/GridEye Data Center

The FNET/GridEye data center is capable of managing, technically processing, and safely archiving the measurements in a systematic way. It has a multi-layer structure as shown in Fig.4 [79].
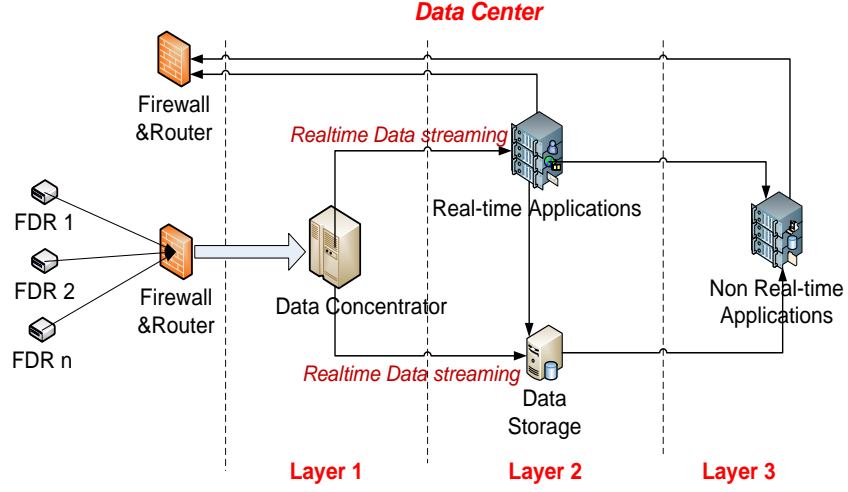
Fig. 4. *The FNET/GridEye data centre structure*

The first layer of the data centre is the data concentrator, in which TCP/IP data packages are extracted, interpreted, error-checked, time-aligned, and then streamed into the subsequent layer. The second layer includes two agents: the real-time application agent and the data storage agent. Various real-time application modules are running on the real-time application agent to monitor power grid dynamic behaviours based on streaming data. For example, on this agent, the real-time event detection module monitor disturbances on the interconnection scale and sends out event alerts to system operators. Meanwhile, the data storage agent archives phasor measurement data streams and outputs from the real-time application agent for off-line applications. All data are archived in an efficient format to preserve data integrity while saving space. In the third layer, the non-real-time application agent runs offline applications to further exploit the archived data [81]. The archived data is a valuable information source for power grid research. For example, the dynamic models of US power grids could be validated through comparing the actual system frequency responses (stored in the archived phasor measurements) with the model-based simulation results [82].

The multi-layer structure of the FNET/GridEye server facilitates efficient concentrating, processing, and archiving wide-area measurements so as to successfully meet the timeliness requirements of various functionalities [41, 83]. Based on the FNET/GridEye platform, a variety of visualization and analytics applications have been developed, and they are widely adopted by the academia, the industry, and government agencies [84]. These applications enable system operators to keep better aware of the spatiotemporal evolvement of power grid dynamics rendered by various disturbances and changing environments.

3. **Disturbance Location Determination Based on Electromechanical Wave Propagation**

Since the interconnection-level power grid is large and the FDR distribution is coarse, the FDR measurement in disturbance location is not available except for those cases in which disturbances happen in FDR-installed locations. A disturbance of the power grid results to speed changes of generator rotors, similar to the phenomenon of wave dissemination on a water surface. The speed of generator rotors, which is denoted by the frequency measurement, is a good indicator of the electromechanical wave impact. To determine the disturbance location, the proposed method uses frequency measurements of FDRs sparsely distributed in a wide area at the distribution level. Besides, this method adopts Delaunay triangulation and bicubic 2D interpolation to locate disturbance in a more accurate way. The workflow of the proposed method includes the following steps:

1) align the frequency measurement based on the GPS timestamp;
2) filter and interpolate the frequency measurement to eliminate aliasing and reconstruct frequency profile;
3) extract the relative arrival time;
4) perform Delaunay triangulation of FDR GPS coordinates;
5) interpolate the response time in the spatial domain using bicubic 2D interpolation;
6) locate the disturbance by searching the minimum relative arrival time;
7) Validate measurements to eliminate impact from bad data; and
8) calculate the propagation speed distribution.
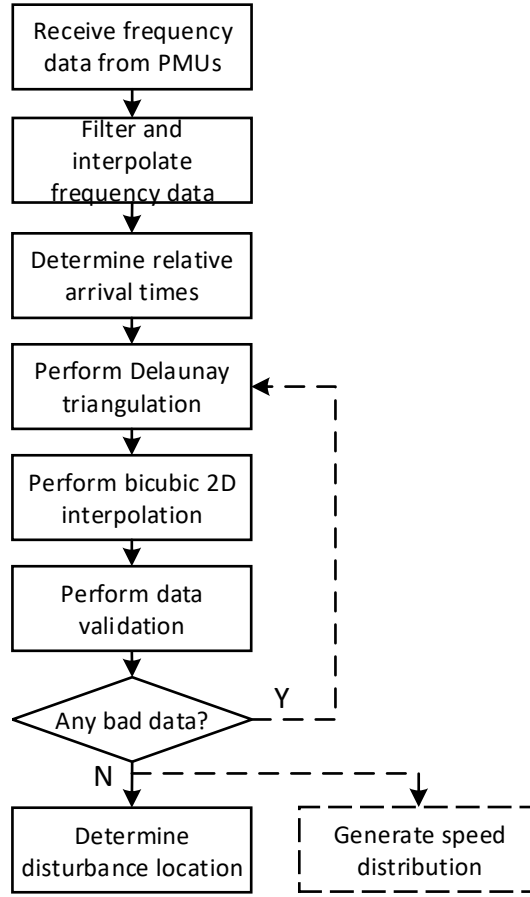
The structure of the workflow is shown in Fig. 5.

Fig. 5. *The flow chart of the disturbance location method*

3.1. Frequency measurement filtering, interpolation, and relative arrival time

FDRs measure the frequency at different locations during a power grid disturbance. The frequency data during a disturbance event is filtered with a moving average filter to remove the high frequency noise. Thus, an equivalent form of the average filter for frequency measurement is defined as:

$$\bar{f} = \frac{1}{N}\sum_{i=1}^{N} f_i \tag{1}$$

where *N* is the size of the moving window. For the reporting rate of ten measurements per second in the current FNET/GridEye system, *N* is set to 5. After filtering, the frequency measurements are interpolated before obtained the time delay of arrival for each FDR. The aim of implementing interpolation is to reconstruct the frequency during the periods between the reporting time snapshot, so that a better estimation of the arrival time can be obtained. In this paper, linear interpolation is applied.

As an example, a generation trip disturbance happened at 13:48:05 (UTC) on Nov. 21st, 2014. During this event, 61 FDRs were streaming data at different locations of the U.S. Eastern Interconnection (EI) power grid. The frequency dropped from 60.005Hz to around 59.975Hz through an "L" profile, which is a typical

frequency response of a generation trip disturbance. Fig. 6 shows the filtered and interpolated frequency data of the detected disturbance event from multiple FDR units. The start time of the decrease of frequency relates to the distance of the FDR and the disturbance location. Those FDR units that are closer to the disturbance source have sharper and early decrease in frequency measurement. To calculate the relative arrival time, a threshold of frequency f_T is applied. Subroutines are developed to detect the disturbance, determined the threshold f_T and the common reference time t_R for a specific disturbance automatically. Determining the threshold value f_T involves three steps.

    1) Calculate the system average frequency;

    2) Calculate the ROCOF (rate of change of frequency) of the average frequency;

    3) Determine the event start time based on ROCOF; and

    4) f_T = frequency at the event start time $- \Delta f$.

Δf is the frequency deviation threshold. This value can be easily determined by examining typical disturbances in a specific system. For EI, this value is 0.005Hz. In step 3, the event start time is determined by confirming that after a timestamp (the event start time), the majority ROCOF values (75% for EI) during a consecutive period (4 second for EI) are larger than a threshold ROCOF (1mHz/s for EI). A majority (75% for EI) of ROCOF passing the threshold is enough to confirm the event occurrence because of the influence of oscillations stirred up by event disturbances. The relative arrival time is then defined as the difference between the common reference time t_R and the time of a FDR's frequency exceeding the threshold. For the case shown in Fig. 6, f_T is calculated to be 60.0014Hz and t_R is selected as18.8s, respectively, as shown in Fig. 7. It is worth noting that the purpose of introducing t_R is to set a common reference of the response time. It does not influence the event location result.
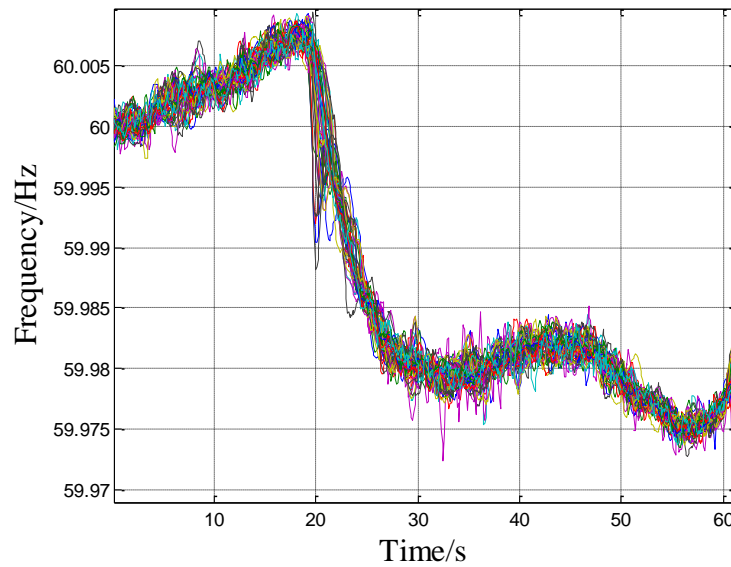

8

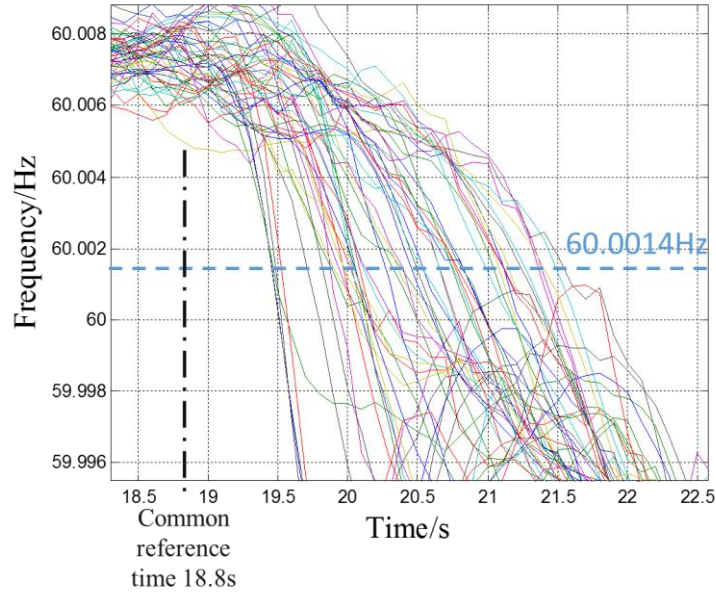**Fig. 6.** *Filtered frequency (5 points median) of the detected disturbance*

Fig. 7. *Relative arrival time*

Table 1 lists the relative arrival time of some FDRs and Fig. 8 graphically shows the relative arrival time of FDRs at different locations. Blue dots represent earlier response time whereas red ones represent relatively later responses. It shows that FDRs in four states: Kansas, Missouri, Arkansas, and Louisiana, had the smallest response time recorded (~0.7s). The New England area, which was remote from the disturbance, had the largest delay of response.

Table 1. Relative arrival time of some FDRs

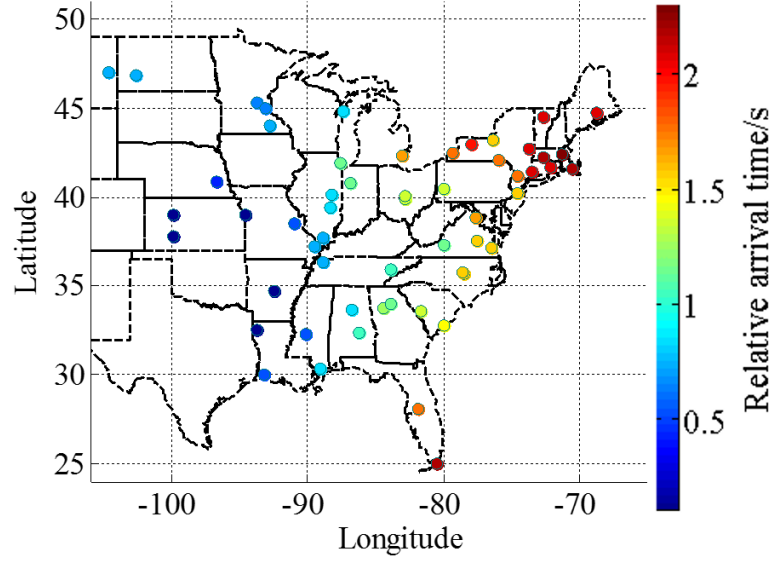| FDR #	FDR Location		Relative Arrival Time (s)
	State	Location (City or Company)	
844	KS	Dodge City	0.7870
941	KS	Wakeeney	0.7608
647	AR	Little Rock	0.7709
979	LA	Shreveport	0.8273
886	MO	Kansas City	0.7595
777	NE	LES	0.9996
756	MO	Franklin	1.1798
1027	MS	Jackson	1.1941
906	TX	Pleasant Hill	1.1252
792	VA	Hay Market	2.1406
1048	NY	Fredonia	2.2970

Fig. 8. *Relative arrival time of FDRs at different locations*

3.2. Delaunay triangulation and bicubic 2D interpolation

Intuitively, the true disturbance location would be in an area that has the minimum relative arrival time. Since the propagation speed is unknown and it may vary with the power grid status, state-of-the-art methods are highly depended on parameters and could not give a unique solution on the location or the start time of a disturbance. In contrast, this method combines Delaunay triangulation and bicubic 2D interpolation to calculate the disturbance location. The proposed approach is parameter-insensitive, robust against parameter errors. Triangulation of FDR locations. Delaunay triangulation partition the area by triangles using existing FDR locations in a nearest neighbour manner, ensuring that no FDR is within the circumcircle of a triangle formed by other three FDRs. In this method, the indicator of whether FDR_i is within the triangle formed by the location of another three FDRs (FDR_A, FDR_B, FDR_C) is $M_{i-A,B,C}$ as shown in (2). This value should be positive for points lying inside the circumcircles when the FDRs at A,B,C are sorted in counter-clockwise. As Delaunay triangulation in a 2D space is a frequently-performed routine, the Association for Computing Machinery (ACM) archives a standard algorithm (Algorithm 872) [85].

$$M_{i-A,B,C} = \begin{vmatrix} lon_A - lon_i & lat_A - lat_i & (lon_A^2 - lon_i^2) + (lat_A^2 - lat_i^2) \\ lon_B - lon_i & lat_B - lat_i & (lon_B^2 - lon_i^2) + (lat_B^2 - lat_i^2) \\ lon_C - lon_i & lat_C - lat_i & (lon_C^2 - lon_i^2) + (lat_C^2 - lat_i^2) \end{vmatrix} \qquad (2)$$

Fig. 9 shows the spatial Delaunay triangulation of FDR locations in the EI power grid. Delaunay triangulation minimizes the maximum angle of all triangulations that connect three FDR locations, allowing the reconstruction of the responses time at locations that have no FDR installed.
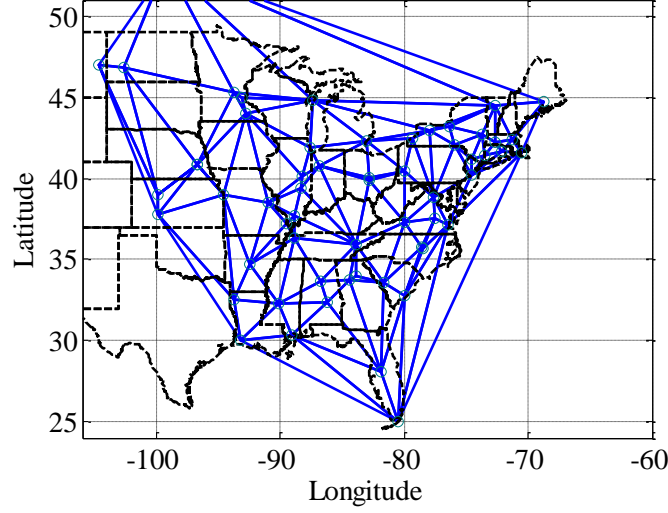
10

Fig. 9. *Delaunay triangulation of FDR locations in the U.S. Eastern Interconnection*

After Delaunay triangulation, this method interpolates the FDR response time using bicubic 2D interpolation for each triangle. For the interpolated arrival time for each triangle has the following form.

$$T(lon, lat) = \sum_{u=0}^{5}\left(\sum_{v=0}^{5-u} a_{u,v} lon^u lat^v\right) \tag{3}$$

where $a_{u,v}$ are the parameters of the polynomial calculated using the triangle-based surface fitting method described in [86], improved from its previous version [86, 87]. An implementation of this algorithm is ACM Algorithm 761 as documented in [88, 89].

Fig. 10 shows the contour map of the bicubic 2D interpolation result. Bicubic 2D interpolation computes a two-dimension cubic function to fit the triangulated response time at the scattered points. The blue areas in Fig. 10 show the locations with smaller response time, indicating locations near the disturbance, whereas the red areas represent significant latency in response due to wave propagation delay.
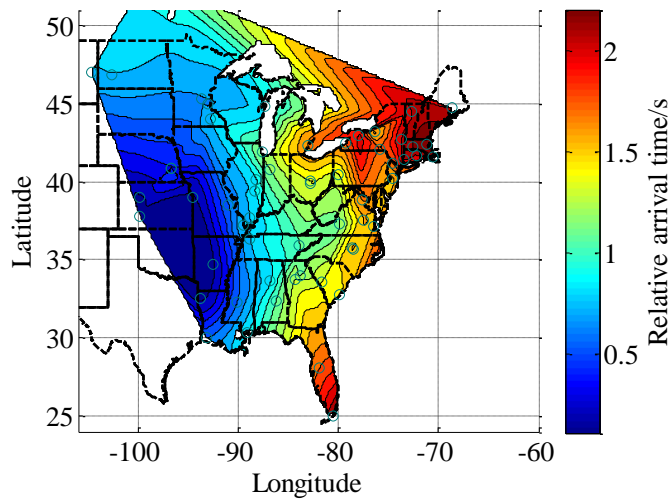

Fig. 10. *The contour map of the time of ROCOF passing a threshold for all FDRs*

3.3. Pinpointing event location and calculating the event start time

The method then scans the mesh grid to look for the point that has the global minimum response time, which is designated as the estimated disturbance location, as shown in Fig. 11. For this case, the computational time consumption to find the disturbance location is 0.461 second using a desktop with a 3.2 GHz CPU. Fig. 12 shows a comparison on the actual and estimated disturbance location. The red, blue, and white dots denote the actual location, the estimated location based on proposed method, the estimated location based on the method in [90]. The distance between the actual and estimated disturbance location using the proposed method is 15.8 miles, while the value is 100.5 miles using the method in [90]. This result indicates the small error of the proposed method.
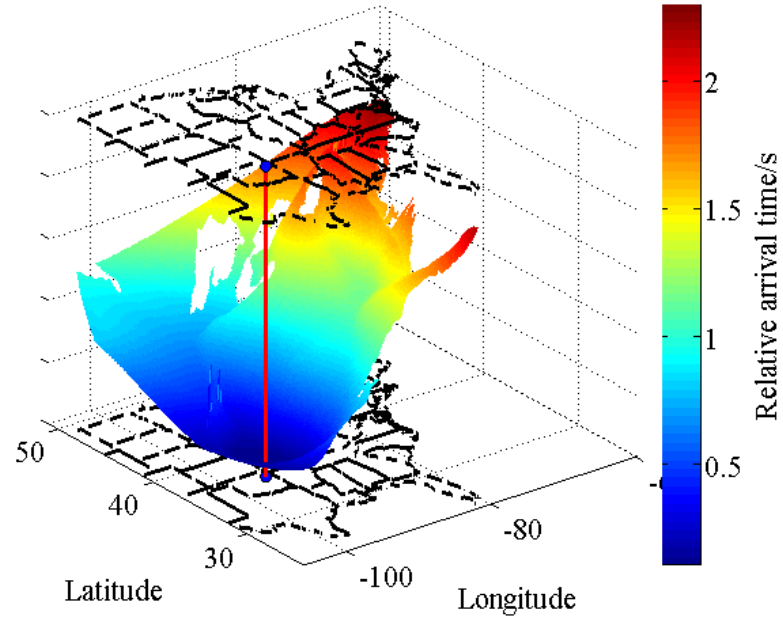

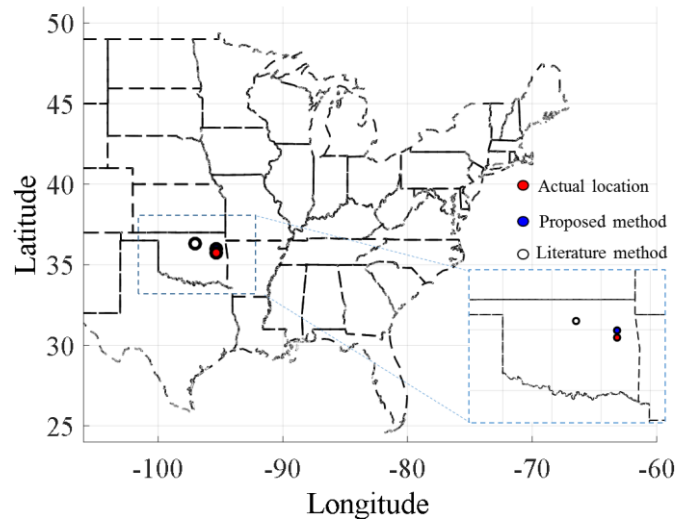**Fig. 11**. *Pinpointing the event location on the contour map*

Fig. 12. *Estimated and actual disturbance location*

Assuming the obtained disturbance location estimation is denoted by $(lon_{event}, lat_{event})$, the response time at this location is denoted by t_{min}. Then the actual disturbance start time is estimated as $t_{event} = t_{min} + t_R$, where t_R is the common time reference for calculating the relative arrival time for all FDRs.

3.4. Data Validation

FDR (or PMU) data may include bad data with some wrong timestamps due to GPS loss, clock error and leap second issues. Therefore, after obtaining the estimated event location and estimated event start time, it is necessary to double check the quality the credibility of the relative arrival time. This validation applies a linear regression method for data validation. The distance between the FDR location and the estimated event location is denoted as

$$D_{(FDR_n, event)} = Distance\{(lon_{FDR_n}, lat_{FDR_n}), (lon_{event}, lat_{event})\} \tag{4}$$

The measured propagation time is calculated as

$$\Delta t_{(FDR_n, event)} = t_{FDR_n} - t_{event} \tag{5}$$

Then the distance and the measured propagation time for each FDR: $\{D_{(FDR_n, event)}, \Delta t_{(FDR_n, event)}\}\big|_{n=1,2,..n}$ are checked using linear regression, assuming the propagation speed is constant, which means the propagation response time delay is proportional to the distance between the FDR location and estimated event location. A threshold is used to find the outliers of the measurements:

$$\left|\Delta t_{(FDR_n, event)} - \Delta t'_{(FDR_n, event)}\right| > \delta_t \tag{6}$$

where $\Delta t'_{(FDR_n, event)}$ is the propagation time from the estimated event location to FDR n obtained from linear regression; δ_t is the tolerance of the deviation between the measurement and the linear regression result. As a typical practice in identifying outliers in linear regression, δ_t is selected as 1.5 times of the interquartile range of near $\Delta t'_{(FDR_n, event)}$. If any FDR is found to be an outlier, then this problematic FDR will be reported to the operator and its data will be deleted before recalculating the event location using Delaunay triangulation and interpolation. An example of the measurement that has the time stamp issue is shown in Fig. 13. It can be seen that the Michigan State has a measurement with wrong timestamp, as marked by the black arrow.
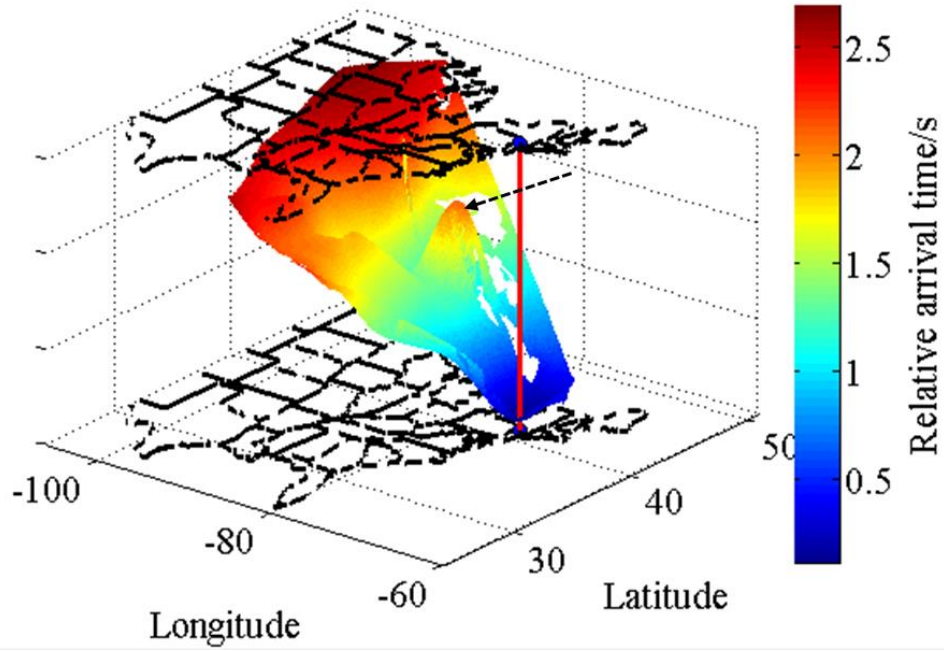
Fig. 13. *Detecting measurement with a time stamp issue in Michigan, U.S.*

To test the robustness of the proposed method, eight events happened during the period from August, 2013 to June, 2015 were tested using the proposed algorithm. The average distance between the estimated location and actual event location is 19.3 miles with a standard deviation of 9.8 miles. Because the maximum angle in the triangle constructed on grid edges will have be larger due to the lack of FDRs on one side, the surface fitting result has relatively larger errors. Therefore, relatively larger errors are often seen for cases in which the actual disturbance location is near the grid edge.

3.5. Electromechanical Wave Propagation Speed Distribution Calculation

Base on the interpolated arrival time distribution $T(lon, lat)$ from validated measurements, the propagation speed can be calculated by the following steps:

1) Calculate the local gradient of the arrival time for each location and for both the longitude and latitude direction, denoted as $\partial T(lon_i, lat_j)/\partial lon$ and $\partial T(lon_i, lat_j)/\partial lat$, respectively.

2) Rescale the directional gradients at each point based on the actual per unit distance in the longitude and latitude side, respectively.

$$\begin{cases} \partial T(lon_i, lat_j)/\partial d_{lon} = (\partial T(lon_i, lat_j)/\partial lon)/UniD_{lon} \\ \partial T(lon_i, lat_j)/\partial d_{lat} = (\partial T(lon_i, lat_j)/\partial lat)/UniD_{lat} \end{cases} \tag{7}$$

3) Obtain the local composite gradient of wave propagation delay based on the two directional gradients.

14

$$\partial T(lon_i, lat_j)/\partial d = \sqrt{(\partial T(lon_i, lat_j)/\partial d_{lon})^2 + (\partial T(lon_i, lat_j)/\partial d_{lat})^2} \qquad (8)$$

4) Inverse the composite gradient to obtain the local propagation speed for location (lon_i, lat_j).

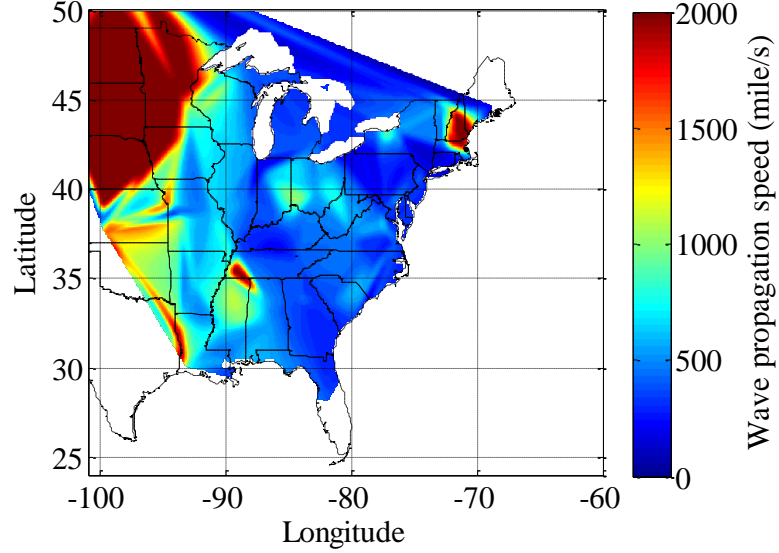$$v_{i,j} = 1/(\partial T(lon_i, lat_j)/\partial d) \qquad (9)$$

Fig. 14. *Wave propagation speed distribution*

Fig. 14 shows the propagation speed distribution. The range of speed distribution (300-800 miles/s) in the east of EI is consistent with sample values observed by utilities in this area [91]. It shows that the propagation speed is higher in the western and lower in the eastern EI. This difference is because the eastern EI has more generation and load, thus having larger inertia than the western part. The higher inertia makes the eastern EI more robust to frequency fluctuations and slows down electromechanical wave propagation. The central EI has a relatively low propagation speed for the same reason. On the contrary, the western EI has less inertia and faster electromechanical wave propagation. Since the proposed method is based on electromechanical wave propagation. The method will work for large load shedding, line trip and faults, as long as the propagation of electromechanical wave propagation can be observed in measurements.

4. Conclusion

This paper demonstrates a new disturbance location determination method implemented on a wide-area frequency monitoring network — FNET/GridEye. Without requiring a pre-determined propagation speed value, the proposed method can accurately pinpoint the disturbance location in the power grid. In addition, this method is robust to timestamp-shifting and measurement error. Based on this method, the real-time distribution of electromechanical wave propagation speed can also be calculated. The proposed method has the generality to be implemented in other WAMSs.

References

1. Amin, S.M. and B.F. Wollenberg, *Toward a smart grid: power delivery for the 21st century.* Power and Energy Magazine, IEEE, 2005. **3**(5): p. 34-41.
2. You, S., et al., *Co-optimizing generation and transmission expansion with wind power in large-scale power grids—Implementation in the US Eastern Interconnection.* Electric Power Systems Research, 2016. **133**: p. 209-218.
3. Hadley, S., et al., *Electric grid expansion planning with high levels of variable generation.* ORNL/TM-2015/515, Oak Ridge National Laboratory, 2015.
4. Guo, J., et al. *An ensemble solar power output forecasting model through statistical learning of historical weather dataset.* in *2016 IEEE Power and Energy Society General Meeting (PESGM).* 2016. IEEE.
5. You, S., *Electromechanical Dynamics of High Photovoltaic Power Grids.* 2017.
6. Sun, K., et al., *A Review of Clean Electricity Policies—From Countries to Utilities.* Sustainability, 2020. **12**(19): p. 7946.
7. Tsai, S.-J., et al., *Frequency sensitivity and electromechanical propagation simulation study in large power systems.* Circuits and Systems I: Regular Papers, IEEE Transactions on, 2007. **54**(8): p. 1819-1828.
8. Phadke, A.G. and J.S. Thorp, *Synchronized phasor measurements and their applications.* 2008: Springer Science & Business Media.
9. Xiao, H., et al., *Data-Driven Security Assessment of Power Grids Based on Machine Learning Approach.* 2020, National Renewable Energy Lab.(NREL), Golden, CO (United States).
10. Wang, J., et al., *Flexible transmission expansion planning for integrating wind power based on wind power distribution characteristics.* J. Electr. Eng. Technol, 2015. **10**: p. 709-718.
11. You, S., et al., *Impact of high PV penetration on the inter-area oscillations in the US eastern interconnection.* IEEE Access, 2017. **5**: p. 4361-4369.
12. Till, A., S. You, and Y. Liu, *Impact of High PV Penetration on Transient Stability—a Case Study on the US ERCOT System.*
13. Hadley, S.W. and S. You, *Influence Analysis of Wind Power Variation on Generation and Transmission Expansion in US Eastern Interconnection.*
14. You, S., et al., *Oscillation mode identification based on wide-area ambient measurements using multivariate empirical mode decomposition.* Electric Power Systems Research, 2016. **134**: p. 158-166.
15. Wang, J., et al., *Long-term maintenance scheduling of smart distribution system through a PSO-TS algorithm.* Journal of Applied Mathematics, 2014. **2014**.
16. Wang, R., et al. *A Novel Transmission Planning Method for Integrating Large-Scale Wind Power.* in *2012 Asia-Pacific Power and Energy Engineering Conference.* 2012. IEEE.
17. You, S., et al. *A Review on Artificial Intelligence for Grid Stability Assessment.* in *2020 IEEE International Conference on Communications, Control, and Computing Technologies for Smart Grids (SmartGridComm).* 2020. IEEE.
18. Lv, C., et al., *Short‐term transmission maintenance scheduling based on the benders decomposition.* International Transactions on Electrical Energy Systems, 2015. **25**(4): p. 697-712.
19. You, S., et al. *Ring-down oscillation mode identification using multivariate empirical mode decomposition.* in *2016 IEEE Power and Energy Society General Meeting (PESGM).* 2016. IEEE.
20. Liu, Y. *A US-wide power systems frequency monitoring network.* in *Power Systems Conference and Exposition, 2006. PSCE'06. 2006 IEEE PES.* 2006. IEEE.
21. Wang, W., et al. *Advanced synchrophasor-based application for potential distributed energy resources management: key technology, challenge and vision.* in *2020 IEEE/IAS Industrial and Commercial Power System Asia (I&CPS Asia).* 2020. IEEE.
22. Cui, Y., S. You, and Y. Liu. *Ambient Synchrophasor Measurement Based System Inertia Estimation.* in *2020 IEEE Power & Energy Society General Meeting (PESGM).* 2020. IEEE.
23. You, S., et al. *Data architecture for the next-generation power grid: Concept, framework, and use case.* in *2015 2nd International Conference on Information Science and Control Engineering.* 2015. IEEE.
24. Zhao, J., et al. *Data quality analysis and solutions for distribution-level PMUs.* in *2019 IEEE Power & Energy Society General Meeting (PESGM).* 2019. IEEE.
25. Liu, Y., et al., *A distribution level wide area monitoring system for the electric power grid–FNET/GridEye.* IEEE Access, 2017. **5**: p. 2329-2338.
26. Tong, N., et al. *Dynamic Equivalence of Large-Scale Power Systems Based on Boundary Measurements.* in *2020 American Control Conference (ACC).* 2020. IEEE.
27. Li, J., et al., *A fast power grid frequency estimation approach using frequency-shift filtering.* IEEE Transactions on Power Systems, 2019. **34**(3): p. 2461-2464.
28. You, S., et al. *FNET/GridEye for Future High Renewable Power Grids—Applications Overview.* in *2018 IEEE PES Transmission & Distribution Conference and Exhibition-Latin America (T&D-LA).* 2018. IEEE.
29. Yao, W., et al., *GPS signal loss in the wide area monitoring system: Prevalence, impact, and solution.* Electric Power Systems Research, 2017. **147**: p. 254-262.
30. Liu, S., et al., *Impact of simultaneous activities on frequency fluctuations—comprehensive analyses based on the real measurement data from FNET/GridEye.* CSEE Journal of Power and Energy Systems, 2020.
31. Wang, W., et al., *Information and Communication Infrastructures in Modern Wide-Area Systems.* Wide Area Power Systems Stability, Protection, and Security: p. 71-104.
32. Zhang, X., et al. *Measurement-based power system dynamic model reductions.* in *2017 North American Power Symposium (NAPS).* 2017. IEEE.
33. Liu, S., et al., *Model-free Data Authentication for Cyber Security in Power Systems.* IEEE Transactions on Smart Grid, 2020.
34. Wu, L., et al. *Multiple Linear Regression Based Disturbance Magnitude Estimations for Bulk Power Systems.* in *2018 IEEE Power & Energy Society General Meeting (PESGM).* 2018. IEEE.
35. You, S., et al., *Power system disturbance location determination based on rate of change of frequency.* 2019, Google Patents.
36. Liu, Y., et al. *Recent application examples of FNET/GridEye.* in *2018 IEEE 12th International Conference on Compatibility, Power Electronics and Power Engineering (CPE-POWERENG 2018).* 2018. IEEE.
37. Liu, Y., et al., *Recent developments of FNET/GridEye—A situational awareness tool for smart grid.* CSEE Journal of Power and Energy Systems, 2016. **2**(3): p. 19-27.
38. Liu, Y., S. You, and Y. Liu, *Smart transmission & wide area monitoring system.* Communication, Control and Security for the Smart Grid, 2017.
39. Yao, W., et al., *Source location identification of distribution-level electric network frequency signals at multiple geographic scales.* IEEE Access, 2017. **5**: p. 11166-11175.
40. Wu, L., et al. *Statistical analysis of the FNET/grideye-detected inter-area oscillations in Eastern Interconnection (EI).* in *2017 IEEE Power & Energy Society General Meeting.* 2017. IEEE.
41. You, S., et al. *A survey on next-generation power grid data architecture.* in *2015 IEEE Power & Energy Society General Meeting.* 2015. IEEE.
42. Zhang, X., et al. *US eastern interconnection (EI) model reductions using a measurement-based approach.* in *2018 IEEE/PES Transmission and Distribution Conference and Exposition (T&D).* 2018. IEEE.

43. You, S., et al., *Wide-area monitoring and anomaly analysis based on synchrophasor measurement*, in *New Technologies for Power System Operation and Analysis*. Elsevier. p. 143-161.
44. Guo, J., *Data Analytics and Application Developments Based on Synchrophasor Measurements*. 2016.
45. You, S., et al. *Ring-down oscillation mode identification using multivariate empirical mode decomposition*. in *Proc. 2016 IEEE Power and Energy Society General Meeting*. 2016.
46. Chai, J., *Wide-Area Measurement-Based Applications for Power System Monitoring and Dynamic Modeling*. 2016.
47. Hwang, J.K. and Y. Liu, *Discrete Fourier transform-based parametric modal identification from ambient data of the power system frequency*. IET Generation, Transmission & Distribution, 2016. **10**(1): p. 213-220.
48. Su, Y., et al., *Adaptive PV Frequency Control Strategy Based on Real-time Inertia Estimation*. IEEE Transactions on Smart Grid, 2020.
49. Li, H., et al., *Analytic analysis for dynamic system frequency in power systems under uncertain variability*. IEEE Transactions on Power Systems, 2018. **34**(2): p. 982-993.
50. You, S., et al., *Comparative assessment of tactics to improve primary frequency response without curtailing solar output in high photovoltaic interconnection grids*. IEEE Transactions on Sustainable Energy, 2018. **10**(2): p. 718-728.
51. Tan, J., et al. *Developing High PV Penetration Case for Frequency Response study of U.S. Western Interconnection*. in *The 9th Annual IEEE Green Technologies Conference*. March 2017. Denver, Colorado: IEEE.
52. You, S., et al. *Energy Storage for Frequency Control in High Photovoltaic Power Grids*. in *IEEE EUROCON 2019-18th International Conference on Smart Technologies*. 2019. IEEE.
53. Yao, W., et al., *A fast load control system based on mobile distribution-level phasor measurement unit*. IEEE Transactions on Smart Grid, 2019. **11**(1): p. 895-904.
54. Yuan, Z., et al. *Frequency control capability of Vsc-Hvdc for large power systems*. in *2017 IEEE Power & Energy Society General Meeting*. 2017. IEEE.
55. Liu, Y., et al., *Frequency response assessment and enhancement of the US power grids toward extra-high photovoltaic generation penetrations—An industry perspective*. IEEE Transactions on Power Systems, 2018. **33**(3): p. 3438-3449.
56. You, S., et al., *Non-invasive identification of inertia distribution change in high renewable systems using distribution level PMU*. IEEE Transactions on Power Systems, 2017. **33**(1): p. 1110-1112.
57. Tan, J., et al. *Frequency Response Study of US Western Interconnection under Extra-High Photovoltaic Generation Penetrations*. in *2018 IEEE Power & Energy Society General Meeting (PESGM)*. 2018. IEEE.
58. Sun, K., et al., *Frequency secure control strategy for power grid with large-scale wind farms through HVDC links*. International Journal of Electrical Power & Energy Systems, 2020. **117**: p. 105706.
59. You, S., et al. *Impact of high PV penetration on US eastern interconnection frequency response*. in *2017 IEEE Power & Energy Society General Meeting*. 2017. IEEE.
60. Till, J., et al. *Impact of High PV Penetration on Voltage Stability*. in *2020 IEEE/PES Transmission and Distribution Conference and Exposition (T&D)*. 2020. IEEE.
61. Yuan, H., et al. *Machine Learning-Based PV Reserve Determination Strategy for Frequency Control on the WECC System*. in *2020 IEEE Power & Energy Society Innovative Smart Grid Technologies Conference (ISGT)*. 2020. IEEE.
62. You, S., et al. *Real-time Frequency Response Reserve based on System Inertia*. in *2020 IEEE/PES Transmission and Distribution Conference and Exposition (T&D)*. 2020. IEEE.
63. Liu, Y., S. You, and Y. Liu, *Study of wind and PV frequency control in US power grids—EI and TI case studies*. IEEE power and energy technology systems journal, 2017. **4**(3): p. 65-73.
64. You, S., et al. *US Eastern Interconnection (EI) Electromechanical Wave Propagation and the Impact of High PV Penetration on Its Speed*. in *2018 IEEE/PES Transmission and Distribution Conference and Exposition (T&D)*. 2018. IEEE.
65. Wang, W., et al., *Multiple event detection and recognition through sparse unmixing for high-resolution situational awareness in power grid*. IEEE Transactions on Smart Grid, 2014. **5**(4): p. 1654-1664.
66. Guo, J., et al., *Design and implementation of a real-time off-grid operation detection tool from a wide-area measurements perspective*. IEEE Transactions on Smart Grid, 2015. **6**(4): p. 2080-2087.
67. Gardner, R.M., Z. Zhong, and Y. Liu, *Location determination of power system disturbances based on frequency responses of the system*. 2010, Google Patents.
68. Lapinski, S. and D. Alphenaar, *Method and system for AC power grid monitoring*. 2006, Google Patents.
69. Gardner, R.M., J.K. Wang, and Y. Liu. *Power system event location analysis using wide-area measurements*. in *2006 IEEE Power Engineering Society General Meeting*. 2006. IEEE.
70. You, S., et al., *Power System Disturbance Location Determination Based on Rate of Change of Frequency*. 2016: U.S.
71. Lee, D.-T. and B.J. Schachter, *Two algorithms for constructing a Delaunay triangulation*. International Journal of Computer & Information Sciences, 1980. **9**(3): p. 219-242.
72. Shewchuk, J.R., *Triangle: Engineering a 2D quality mesh generator and Delaunay triangulator*, in *Applied computational geometry towards geometric engineering*. 1996, Springer. p. 203-222.
73. Watson, D., *Contouring: a guide to the analysis and display of spatial data*. Vol. 10. 2013: Elsevier.
74. You, S., et al. *Impact of High PV Penetration on U.S. Eastern Interconnection Frequency Response*. in *Power and Energy Society General Meeting (PESGM), 2017*. 2017. IEEE.
75. Hadley, S.W., et al., *Electric Grid Expansion Planning with High Levels of Variable Generation*. ORNL/TM-2015/515, Oak Ridge National Laboratory, 2015.
76. Xu, C., et al., *Practical issues in frequency disturbance recorder design for wide-area monitoring*. Electrical Power Quality and Utilisation. Journal, 2005. **11**(1): p. 69-76.
77. Liu, Y., et al., *Wide-Area Measurement System Development at the Distribution Level: an FNET/GridEye Example*. Power Delivery, IEEE Transactions on, 2016.
78. Wang, L., et al. *Frequency disturbance recorder design and developments*. in *Power Engineering Society General Meeting, 2007. IEEE*. 2007. IEEE.
79. Zhang, Y., et al., *Wide-area frequency monitoring network (FNET) architecture and applications*. Smart Grid, IEEE Transactions on, 2010. **1**(2): p. 159-167.
80. Culliss, J.A., *A 3rd Generation Frequency Disturbance Recorder: A Secure, Low Cost Synchophasor Measurement Device*. 2015.
81. Liu, L., et al. *Power grid disturbance analysis using frequency information at the distribution level*. in *Smart Grid Communications (SmartGridComm), 2014 IEEE International Conference on*. 2014. IEEE.
82. Yingchen, Z., et al., *Wind Power Plant Model Validation Using Synchrophasor Measurements at the Point of Interconnection*. Sustainable Energy, IEEE Transactions on, 2015. **6**(3): p. 984-992.

83. You, S., et al. *Data Architecture for the Next-Generation Power Grid: Concept, Framework, and Use Case*. in *Information Science and Control Engineering (ICISCE), 2015 2nd International Conference on*. 2015. IEEE.

84. Liu, Y., S. You, and Y. Liu, *Smart Transmission & Wide Area Monitoring System*, in *Communication, Control and Security for the Smart Grid*. 2017, IET.

85. Chernikov, A.N. and N.P. Chrisochoides, *Algorithm 872: Parallel 2D constrained Delaunay mesh generation.* ACM Transactions on Mathematical Software (TOMS), 2008. **34**(1): p. 6.

86. Akima, H., *A method of bivariate interpolation and smooth surface fitting for irregularly distributed data points.* ACM Transactions on Mathematical Software (TOMS), 1978. **4**(2): p. 148-159.

87. Akima, H., *A method of bivariate interpolation and smooth surface fitting for values given at irregularly distributed points*. Vol. 1. 1975: US Department of Commerce, Office of Telecommunications.

88. Akima, H., *Algorithm 761: scattered-data surface fitting that has the accuracy of a cubic polynomial.* ACM Transactions on Mathematical Software (TOMS), 1996. **22**(3): p. 362-371.

89. *ACM Collected Algorithms.* Website: http://calgo.acm.org/.

90. Ye, Y., *Wide-area situational awareness application developments.* 2011.

91. Chakrabortty, A., *Estimation, analysis and control methods for large-scale electric power systems using synchronized phasor measurements*. 2008: ProQuest.